LIGHT CHARGED PARTICLE PRODUCTION INDUCED BY FAST NEUTRONS (E_N = 25-65 MEV) ON ^{59}Co AND ^{nat}Fe

E. Raeymackers, N. Nica,[1]* I. Slypen, S. Benck, J-P. Meulders, V. Corcalciuc*
Institut de Physique Nucléaire, Université Catholique de Louvain, Chemin du Cyclotron 2,B – 1348 Louvain-la-Neuve, Belgium
*Institute of Atomic Physics, PO Box MG6, Heavy Ion Department, Bucharest, Roumania

Abstract

The present paper reports experimental measurements of light charged particle (proton, deuteron, triton and alpha-particle) production induced by fast neutrons (E_n = 25-65 MeV) on ^{59}Co and ^{nat}Fe. Experimental methods and data reduction procedures are shortly discussed. Preliminary double-differential and energy-differential cross-sections are shown, compared to similar results from proton and neutron induced reactions at comparable energies and to theoretical model calculations.

1. Present Address: Texas A&M University, U.S.A.

Introduction

Due to the lack of experimental data concerning the light charged particle production in fast neutron induced nuclear reactions in the energy range 20-100 MeV, systematic measurements have been performed the last ten years at the Louvain-la-Neuve cyclotron CYCLONE. The aim was to provide nuclear information, i.e. experimental cross-sections, in this energy range for several target nuclei, from light (carbon and oxygen) [1-6] to heavy nuclei (bismuth and uranium). [7,8]

Measurements of fast neutron induced reactions have to cope with important technical difficulties like low intensity beams, use of rather thick targets involving important corrections in the spectra, low cross-sections to be measured and therefore, long acquisition time, etc. Consequently, experimental information is rather scarce for neutron energies above 20 MeV. In addition to the basic nuclear physics interest, the neutron induced reactions above 20 MeV are very important for newly developing Accelerator-driven Systems (mainly transmutation of radioactive waste and alternative energy production). Previous experimental results for neutron induced α-particle production on cobalt by direct detection of α-particles (inclusive spectra) were reported at 14 MeV incident neutron energy [9] and more recently, in the neutron energy interval 5-50 MeV. [10]

Experimental results concerning light charged particle production in proton induced reactions are available for iron and neighbouring nuclei such as ^{60}Ni, ^{56}Fe and ^{54}Fe, [11] at comparable incident proton energies (28.8, 38.8 and 61.7 MeV, depending on the target nucleus). Our data together with those of Ref. 11 provide complementary information on nucleon induced light charged particle emission in this mass region and offer a larger base for testing the nuclear models.

In the present contribution, the experimental methods and data reduction procedures are described. While still in progress, the data analysis is well advanced and preliminary results for the two target nuclei are shown compared to similar experimental results from neutron and proton induced reactions and to theoretical model calculations.

Experimental set-up

A 65 MeV proton beam, coming from the cyclotron is sent on a 3 mm thick natural lithium target (94% of ^{7}Li and 6% of ^{6}Li). The ^{7}Li(p,n)Be$_{gs}$ (Q = -1.64 MeV) and ^{7}Li(p,n)Be* (431 keV) reactions produce, at 0° lab., a quasi-monoenergetic beam of neutrons. This neutron beam is characterised by a main peak centred at 62.7 MeV with a full-width-half-maximum (FWHM) of 2 MeV followed by a flat continuum containing 50% of the produced neutrons but with 10 times less neutrons/MeV than in the main peak. The neutron beam is collimated towards the first reaction chamber to which the charged particle detection system is coupled. For a 10 μA current proton beam on the lithium target, about 10^{6} neutrons/s are available at the target location (about 3.5 m downstream the lithium target).

Protons which did not interact with the lithium target are deflected by a magnetic dipole towards a Faraday cup (graphite bloc) where the current is integrated, allowing an on-line monitoring of the beam and providing a relative information on the neutron flux. Upstream the lithium target is placed a beam pick-off supplying a start-signal for a time-of-flight measurement (Figure 1).

Figure 1. **Schematic view of the experimental set-up** (not at the scale)

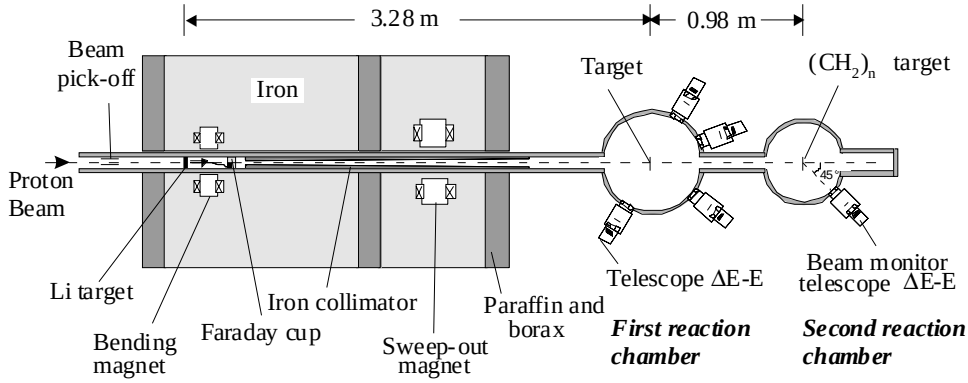

The two targets have surfaces of 6×6 cm² and thickness of 0.4 mm for the cobalt and 0.5 mm for the iron. The thickness was chosen as a compromise between a sufficient count rate and a minimisation of the travel of the produced charged particles through the target material towards the detectors. A 1.0 mm thick polypropylene target and a 0.6 mm deuterated polypropylene target are also used for the calibration and for the absolute normalisation of the spectra. Proton and deuteron peaks resulting from the quasi-elastic scattering of neutrons, are used for the calibration in energy and time of the detectors. Moreover, the n-p scattering provides the reference cross-sections for the absolute normalisation of the experimental data.

The light charged particle detection system consists in the simultaneous use of 6 telescopes placed at 9 laboratory angles around the first reaction chamber: from 20° to 70 ° in step of 10° in the forward hemisphere and at 110°, 140° and 160° in the backward one. The telescopes are of ΔE-E type: i) the ΔE part is a 100 μm thick NE102A plastic scintillator, 4 mm in diameter, coupled to a XP2020 photomultiplier through a light guide, and ii) a E part with a 22 mm thick CsI(Tl) crystal scintillator, 38.1 mm in diameter, directly coupled to a XP2262 photomultiplier. A coincidence between the two parts of the telescope is required to reject an important part of the low-energy background. [12] For each telescope the angular aperture is determined by two collimators to about 2-3°.

The signal given by the CsI(Tl) detector is integrated following 3 time windows adjusted to provide its fast, slow and total component. A time-of-flight (TOF) measurement is also performed for which the "start" is given by the beam pick-off (upstream the Li target) and the "stop" given by the signal of the fast response NE102A plastic scintillator. In this way, to each charged particle event is associated the corresponding TOF.

In the centre of the second reaction chamber (Figure 1) is placed a 1 mm thick polypropylene target at an angle of 45° relative to the incident beam direction. Recoil protons are detected at 45° laboratory by an ΔE-E telescope composed of a 2 mm thick NE102A plastic scintillator (ΔE) and a CsI(Tl) crystal (E). The integration of the recoil proton peak provides a second relative information of the neutron flux. [12] The agreement of the two monitoring systems is very good (2%).

Data reduction procedure

The discrimination of the recorded light charged particles is accomplished by an alternative use of two bi-parametric representations of the detector signals. The first one is a representation of the CsI(Tl) signal in its slow component versus its fast one. The second one is a representation of the ΔE-E signals (Figure 2). While the first representation (slow-fast) allows a good separation of the

different charged particles for most of the energy range, the second one allows the rejection of the low-energy background and refinement of the separation of the particles at low energies. Switching from one representation to the other gives, at the end, a good separation of the charged particles over the whole energy range. Nevertheless, at very low energies (especially for tritons) the separation is very difficult involving analysis uncertainties on the 2-3 last points of the energy spectra.

Knowing the energy calibration, the involved flight distances and the corresponding TOF, an incident neutron energy spectrum is reconstructed for each charged particle species, by associating an incident neutron to each charged particle event. The resulting neutron spectrum is subsequently used for the incident neutron energy selection based on the time resolution in the experiment (0.8 ns). [12]

Such a spectrum is shown in Figure 3 for the protons recorded at 20° lab. with the cobalt target. The insert shows the reconstructed incident neutron spectrum. As an example, the main peak (hatched region) and the 41.0 ± 2.0 MeV energy bin in the continuum (double hatched region) are selected and the corresponding proton spectra induced by these neutrons are shown. In this way, information for several incident neutron energies can be obtained, resulting in a highly consistent set of experimental data. For protons and deuterons this allows the extension of the analysis to about 10 incident neutron energies down to 25 MeV. Because of the low cross-sections for triton and alpha-particle production, the accumulated statistics in the spectra limits this analysis to only 5-7 incident neutron energies and only for forward angles in most of the cases.

Figure 2. **a) Representation of slow vs. fast component of the CsI(Tl) signal**
b) ΔE – E representation

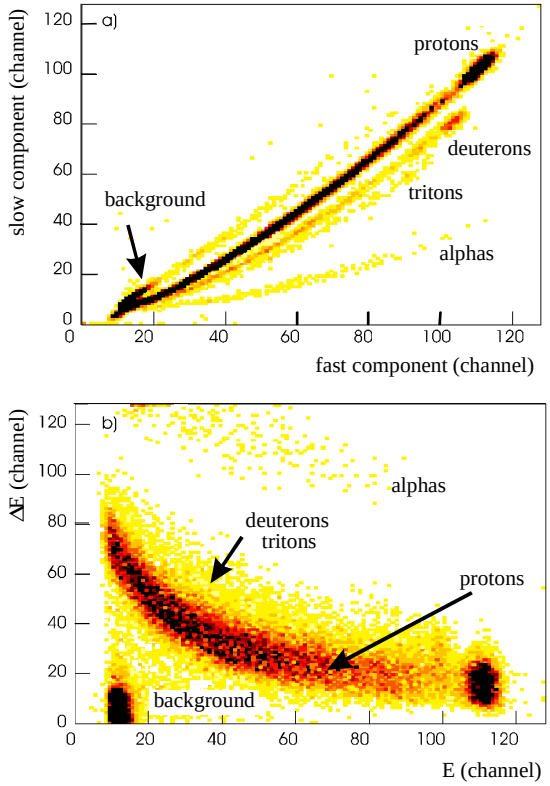

The obtained charged particle energy spectra are normalised to the measured H(n,p) cross-sections [13] at six laboratory angles (20°-70° in step of 10°) with the polypropylene target. In this way six normalisation factors are obtained for each telescope and their mean value is applied for the absolute normalisation. The six normalisation factors for each telescope agree generally within 3%.

Thick target and solid angle corrections to the spectra are calculated with a simulation programme of the experiment. [14] It calculates among other things the attenuation of the produced charged particle flux in the target material and in the ΔE detector. Solid angle calculations are very important because the neutron beam on the target has a diameter of 4 cm.

The overall relative uncertainties of the experimental points in the spectra are about 5.5%, 8.5%, 15% and 25% for respectively p, d, t and α for 62.7 MeV data. They are given mainly by the statistics in the spectra. At lower ejectile energies, the thick target corrections contribute with supplementary uncertainties. For all the other incident neutron energies (continuum), these values are between 2 and 3 times higher as a consequence of a lower incident neutron flux. The uncertainty of the cross-section absolute scale is about 7-8%, due to errors in the measured reference (n,p) cross-sections (5%), beam monitoring (2%), statistics in the H(n,p) recoil proton peak (2-5%), solid angle corrections (1%), number of target nuclei (1%), etc.

From the double-differential cross-sections measured at 9 laboratory angles listed above, it is possible to extrapolate these cross-sections at very forward and backward angles and interpolate them for the missing angles. This is made following an empirical formula of the type $a.exp(b.\cos\theta)$ based on a systematic analysis of the experimental data. [15] Having the complete angular distribution, by respectively angle or energy integration, the energy-differential and angle-differential cross-sections are obtained. A further integration gives the total production cross-section.

Figure 3. **Proton spectrum at 20° laboratory angle**

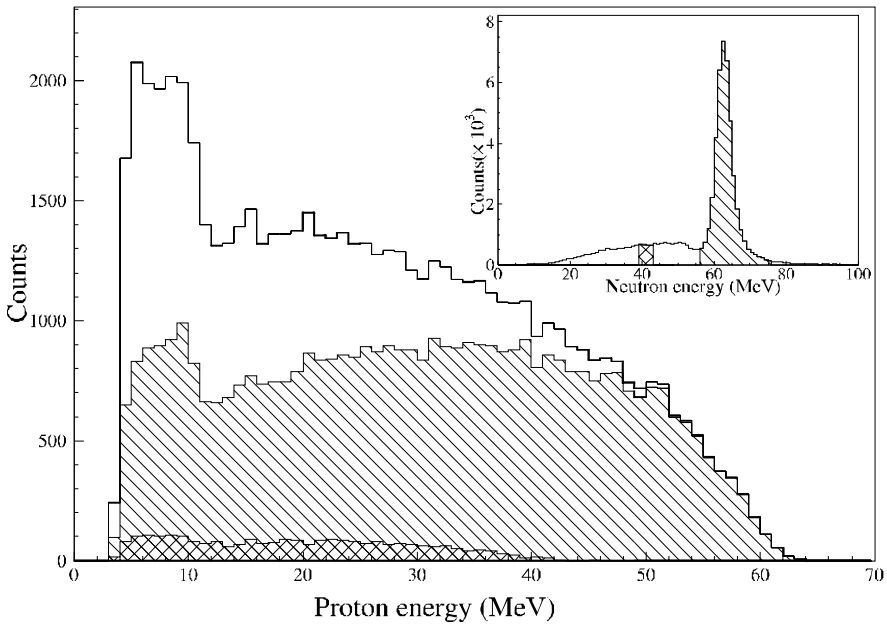

The insert shows the neutron spectrum reconstructed from all protons recorded at this angle. The figure presents the selection of protons induced by neutrons of the main peak (hatched area) and by neutrons of an energy bin in the continuum of the neutron spectrum (double hatched area).

Because the separation was difficult on the entire energy range, the reported cross-sections in the present work for α-particle include the ^{3}He events. Nevertheless, their contribution is much smaller than the one of the ^{4}He, being within the experimental errors. This conclusion is also supported by the theoretical calculations.

Experimental results

Double-differential cross-sections (energy spectra) were measured at the nine laboratory angles listed above and at 10 incident neutron energies (62.7 ± 2.0, 53.5 ± 2.5, 49.0 ± 2.0, 45.0 ± 2.0, 41.0 ± 2.0, 37.5 ± 1.5, 34.5 ± 1.5, 31.5 ± 1.5, 28.5 ± 1.5 and 25.5 ± 1.5 MeV). Figures 4-7 show the double-differential cross-sections for the production of respectively protons, deuterons and tritons (20° lab.) and alpha-particle (30° lab.) for the indicated incident neutron energies.

In all cases, the results on iron and cobalt are in very good agreement as expected for close mass nuclei. For the deuterons, tritons and alpha particles, the agreement between neutron and proton induced reaction results is good, especially in the pre-equilibrium region of the spectra. Differences in the high-energy region are due to a better resolution of the proton experiments and also to the fact that the proton induced reactions lead to other residual nuclei than neutron induced reactions and so, direct processes dominating this region are different. For protons, one can remark a difference between neutron and proton induced reactions. This difference is expected and can be explained by the exciton model. [16]

Some discrepancies occur at very low ejectile energies, even in results coming from more straightforward data handling experiments like the proton induced reactions (data for neighbouring nuclei in Figures 4-7). In our case, for the low energy part of the spectra (mostly the last three points in the spectra of Figures 4-7) there are at least two main difficulties in the data reduction. The outgoing particle energies shown in Figures 4-7 are the produced energies in the reactions and they correspond to 2-7 MeV energies in the detector. For these low values the energy calibration is not very precise. Therefore, slight changes in the particle energy induce important changes in the thick target corrections. On the other hand, in this energy region of the spectra (Figure 2), the discrimination of the charged particle species is not very good (worst example is the separation of deuterons from tritons).

The comparison between neutron induced alpha-particle production results of present work and those of Ref. 10 shows large differences between the two experiments. Due to saturation above 22 MeV ejectile energy in Ref. 10, there are no data points in the spectra to compare with. At low ejectile energy, results of present work indicate the presence of the Coulomb barrier at about 12 MeV while in Ref. 10, large cross-sections were measured down to 4 MeV. The total cross-sections reported in Ref. 10 are therefore 3 to 4 times higher than those of the present work are.

All the theoretical calculations shown in the present paper are done for the cobalt nucleus. The GNASH code calculations [17] are in good agreement with the experimental data for proton and alpha-particle production (except for the 53.5 MeV incident neutron energy) and in fair agreement with the deuteron data. Calculated triton production is 2-3 times lower than the experimental results. The intranuclear cascade model INCL3 [18] calculates only the emission of nucleons. The agreement between calculations and experimental results for protons is very good for incident energies above 40 MeV. Below, the agreement is fair but it must be pointed out that the intranuclear cascade model is expected to work well for energies above 100 MeV.

Figures 4-5. **Double-differential cross-sections for respectively 59Co(n,px) and 59Co(n,dx) reactions (open circles) and for natFe(n,px) and natFe(n,dx) (full triangles) at 20° lab. for the indicated incident neutrons energies**

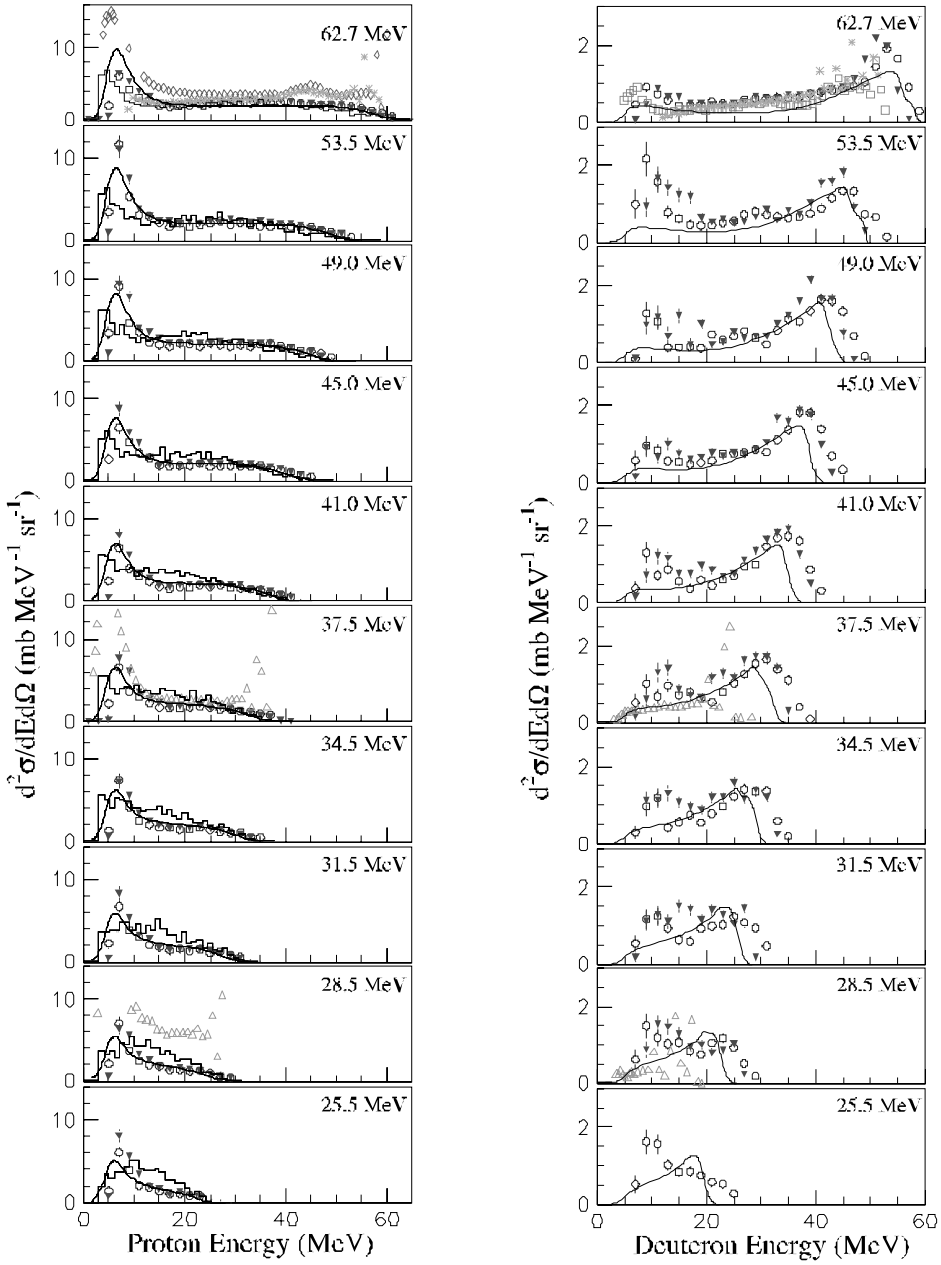

Corresponding data from proton induced reactions for ^{60}Ni (61.7 MeV, diamonds), ^{56}Fe (61.5 MeV, 20° lab., stars; 61.5 MeV, 22° lab., squares) and ^{54}Fe (38.8 and 28.8 MeV, at respectively 20° and 15°, open triangles). INCL3 calculations [18] are presented as histograms while GNASH calculations [17] as continuous lines. Some points of proton induced experiments have been cut because they were out of scale.

The results on cobalt and iron are in excellent agreement. They are also in very good agreement with data from proton induced reactions, except for tritons. Intranuclear cascade model calculations describe quite well the experimental data for the proton emission, especially in the pre-equilibrium region. The GNASH calculations describe well the data for all four particles. Nevertheless, for α-particles the GNASH code calculations agree with the data of Ref. 10 in the low energy part of the spectra.

Figures 6-7. **Double-differential cross-sections for respectively ^{59}Co(n,tx) and ^{59}Co(n,αx) reactions (open circles) and for ^{nat}Fe(n,αx) only (full triangles) at 20° lab. for tritons, 30° lab. for α and for the indicated incident neutrons energies**

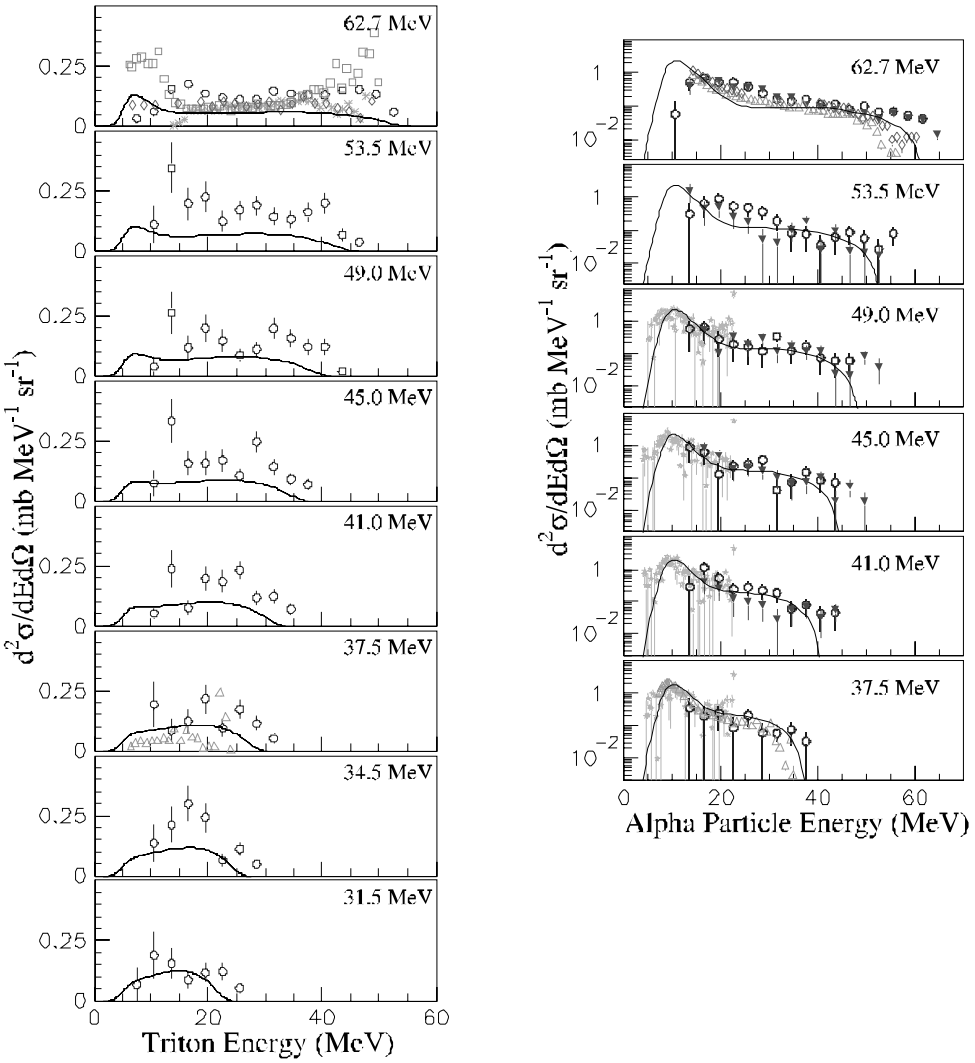

Corresponding data from proton induced reactions for ^{60}Ni (61.7 MeV, 20° lab. for tritons, 25° lab. for α, diamonds), ^{56}Fe (61.5 MeV, 20° lab., full stars; 61.5 MeV, 22° lab., squares) and ^{54}Fe (38.8°, open triangles). Data for ^{59}Co(n,αx) at 30° lab. of Ref. 10 are indicated as open stars. INCL3 calculations are presented as histograms while GNASH calculations as continuous lines.

Figure 8 shows, the energy-differential cross-sections for the emission of the four particles at 62.7 MeV incident neutron energy. Symbols are consistent with those used in Figures 4-7.

Figure 8. **Energy-differential cross-sections for the four particles on ^{59}Co and on ^{nat}Fe at 62.7 MeV incident neutron energy**

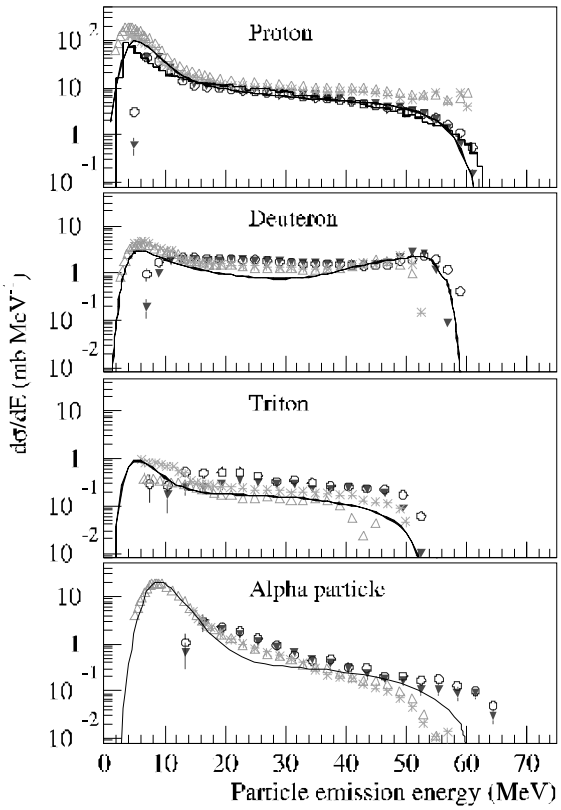

Symbols are consistent with those used in Figures 4-7.

Conclusions

In the present contribution, preliminary experimental results for light charged particle production in fast neutron (25-65 MeV) induced reactions on ^{59}Co and ^{nat}Fe are reported. Experimental methods and the data reduction procedures are shortly discussed and illustrated.

Experimental results are shown for double-differential ($d^2\sigma/d\Omega dE$) and energy-differential ($d\sigma/dE$) cross-sections and they are compared to literature data from corresponding proton and neutron induced reactions. Generally there is a good agreement with data from proton induced reactions. Nevertheless, our alpha-particle spectra for cobalt show important differences in the low energy part of the spectra relatively to the previous published ones from neutron induced reactions.

Both theoretical calculations (GNASH nuclear data code and intranuclear cascade model) describe well the experimental spectra. Calculated alpha-particle spectra by GNASH code predict important low energy cross-sections not observed in our experiment.

Acknowledgements

We acknowledge support of the Institut Interuniversitaire des Sciences Nucléaires, Belgium and partly the European Economic Community (contract FIKW-CT-2000-00031). Dr. N. Nica thanks the Belgian French Community for partly financing his stay at the Université catholique de Louvain (L.L.N.). Dr. S. Benck thanks the Fonds National de la Recherche Scientifique, Belgium for the financial support as a Scientific Collaborator (chargé de recherches). We thank Prof. J. Cugnon for making available the Liege intranuclear cascade code (INCL3).

REFERENCES

[1] I. Slypen, V. Corcalciuc and J.P. Meulders, Phys. Rev. C51, (1995) 1303.

[2] I. Slypen, V. Corcalciuc, J.P. Meulders, M.B. Chadwick, Phys. Rev. C53, (1997) 1309.

[3] I. Slypen, S. Benck, J.P. Meulders, V. Corcalciuc, Nucl. Phys. A671, (2000) 3.

[4] C. Dufauquez, I. Slypen, S. Benck, J.P. Meulders, V. Corcalciuc, Nucl. Phys. A671, (2000) 20

[5] S. Benck, I. Slypen, J.P. Meulders, V. Corcalciuc, Eur. Phys. J. A3, (1998) 149.

[6] S. Benck, I. Slypen, J.P. Meulders, V. Corcalciuc, Eur. Phys. J. A3, (1998) 159.

[7] E. Raeymackers, I. Slypen, S. Benck, J.P. Meulders, N. Nica, V. Corcalciuc, Int. Conf. On Nucl. Data for Science and Tech., 2001 Oct 7-12, Tsukuba, Japan.

[8] S. Benck, E. Raeymackers, I. Slypen, J.P. Meulders, V. Corcalciuc, Int. Conf. On Nucl. Data for Science and Tech., 2001 Oct 7-12, Tsukuba, Japan.

[9] R. Fisher, G. Traxler, M. Uhl, H. Vonach, P. Mayer-Komor, Phys. Rev. C34, 460 (1986).

[10] S.M. Grimes, C.E. Brent, F.C. Goeckner, F.B. Bateman, M.B. Chadwick, R.C. Haight, T.M. Lee, S.M. Sterbenz, P.G. Young, O.A. Watson, H. Vonach, Nucl. Sci. Eng. 124, 27 (1996).

[11] F.E. Bertrand and R.W. Peelle, Phys. Rev. C8, 1045 (1973).

[12] F.E. Bertrand and R.W. Peelle, Oak Ridge Report, ORNL-4799 (1973).

[13] I. Slypen, V. Corcalciuc, A. Ninane and J.P. Meulders, Nucl. Instrum. Methods A337, 431 (1994).

[14] S. Benck, I. Slypen, V. Corcalciuc and J.P. Meulders, Nucl. Phys. A615, 220 (1997).

[15] I. Slypen, V. Corcalciuc and J.P. Meulders, Nucl. Instrum. Methods B88, 275 (1994).

[16] C. Kalbach, Phys. Rev. C37, 2350 (1988).

[17] S. Benck, I. Slypen, J.P. Meulders, V. Corcalciuc, M.B. Chadwick, P.G. Young, A.J. Koning Phys. Rev. C58, 1558 (1998).

[18] P.G. Young, E.D. Arthur, M.B. Chadwick, LANL Report No. LA-12343-MS , (1992), GNASH-FKK version gn9cp0, PSR-0125, programme received from NEA Data Bank (1999).

[19] J. Cugnon, Nucl. Phys. A462, 751 (1987).

[20] J. Cugnon, C. Volant, S. Vuillier, Nucl. Phys. A620, 475 (1997).